Inorganic Chemistry

Article

pubs.acs.org/IC

Distal Histidine Modulates the Unusual O-Binding of Nitrite to Myoglobin: Evidence from the Quantum Chemical Analysis of EPR Parameters

Mahesh Sundararajan*,† and Frank Neese‡

†Theoretical Chemistry Section, Bhabha Atomic Research Centre, Mumbai 400 085, India

‡Max-Planck-Institut für Chemische Energiekonversion, Stiftstrasse 34-36, D-45470 Mülheim an der Ruhr, Germany

Supporting Information

ABSTRACT: Nitrite ligand can coordinate with the transition metal through either N- or O-, which is known as linkage isomerism and is believed to occur in metalloproteins. In contrast to the commonly found N-binding motif of nitrite to iron in synthetic models, the less commonly observed O-binding of nitrite to myoglobin (Copeland, D. M.; Soares, A. S.; West, A. H.; Richter-Addo, G. B. *J. Inorg. Biol. Chem.* **2006**, *100*, 1413−1425) and hemoglobin (Yi, J.; Safo, M. K.; Richter-Addo, G. *Biochemistry*, **2008**, *47*, 8247−8249) reported by Richter-Addo and co-workers is intriguing. On the basis of site-directed mutagenesis studies, it was argued that the distal histidine modulates this unique binding. However, EPR measurements on nitrite binding to methemoglobin could not rule out the possibility of N-bound species to low spin ferric iron. Given to the very similar active sites, there exists a controversy within the two powerful experimental techniques in identifying the coordination motif of nitrite to myoglobin, which is central to understanding the denitrification mechanism. Herein, we report the computation of spin Hamiltonian EPR parameters of different linkage isomers of nitrite bound myoglobin using wave function based "ab initio" and density functional theories to shed light on the binding motif of nitrite to ferric iron. Our predicted spin Hamiltonian parameters agree closely with the experimental EPR data, which provides strong support for the crystallographically implied O-binding to the low-spin ferric heme. This unique O-binding of nitrite to iron is modulated by the distal histidine whose contributions to the active site electronic structure have been successfully quantified. Our quantum chemical insights on the electronic structure of this intermediate are crucial for understanding the structure−function relationship of other metal-nitrite species found in various metalloenzymes.

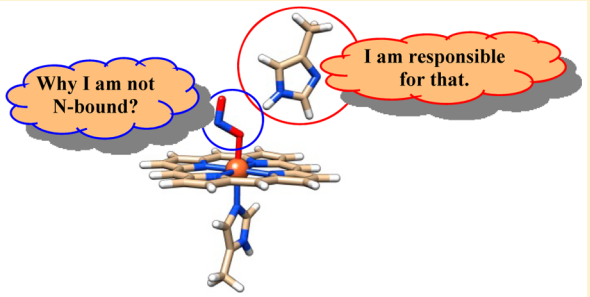

1. INTRODUCTION

The discovery of coordination compounds by Werner have led to many intriguing chemical structures and stereochemical properties of metal complexes.[1] Of these, nitrite anion binding to cobalt (Co^{3+}) led to the formation of red and yellow colored complexes. The structural origin of these complexes was first explained by Werner and later became commonly known as nitro-nitrito linkage isomerism.[1b] The coordination mode of nitrite to metal centers is either commonly found nitro ($-NO_2^-$) or the less common nitrito ($-ONO^-$) variant.[2,3] Linkage isomerism is also known for other ligands such as thiocyanate (SCN),[3a] nitric oxide (NO),[3b] and sulfur monoxide (SO)[3c] and has been observed in a variety of coordination complexes.[3d] Furthermore, $-NO_2^-/-ONO^-$ linkage isomerism also plays a vital role in microbial denitrification, a biochemical process that is efficiently catalyzed by a variety of metalloenzymes.[4] For example, nitrite binds to copper (Cu^{2+}) and molybdenum (Mo^{4+}) through bidentate and monodentate nitrito motifs, whereas in cytochrome *d*-containing proteins (cd1-NiR) and nitrite coordinate to the Fe-heme through nitrogen.[4a]

Iron-nitrite and nitrosyls are commonly formed intermediates in the reaction mechanisms of biochemical reactions whose geometric and electronic structures have attracted chemists for many decades.[5,6] In contrast to a majority of inorganic synthetic models, Copeland et al.,[7a] reported the unusual O-binding of nitrite (ONO) to low spin ($S = 1/2$) ferric (Fe^{3+}) myoglobin through an X-ray crystallographic technique. On the basis of site-directed mutagenesis, it was argued that the distal His64 modulates the uncommon ONO binding to hemes.[7b] Very recently, Yi et al., reported that even reduced hemes (Fe^{2+})[7c] and other metal mutants[7d] such as cobalt and manganese bind through the −ONO motif. Further, even in hemoglobin Yi et al. found the uncommon O-binding to nitrite.[7e]

Thus, to understand the unique electronic structures of low spin ferric hemes, spectroscopic methods such as infrared (IR), Mössbauer (MB), and EPR spectroscopy have always played a dominant role in metallobiochemistry, as in the pioneering model chemistry work of Ford,[8] Scheidt,[9] and Walker.[10] On the

Received: March 11, 2015
Published: July 14, 2015

DOI: 10.1021/acs.inorgchem.5b00557
Inorg. Chem. 2015, 54, 7209−7217

Scheme 1. Possible Mechanistic Consequences of Nitrite-Nitrito Linkage Isomerism

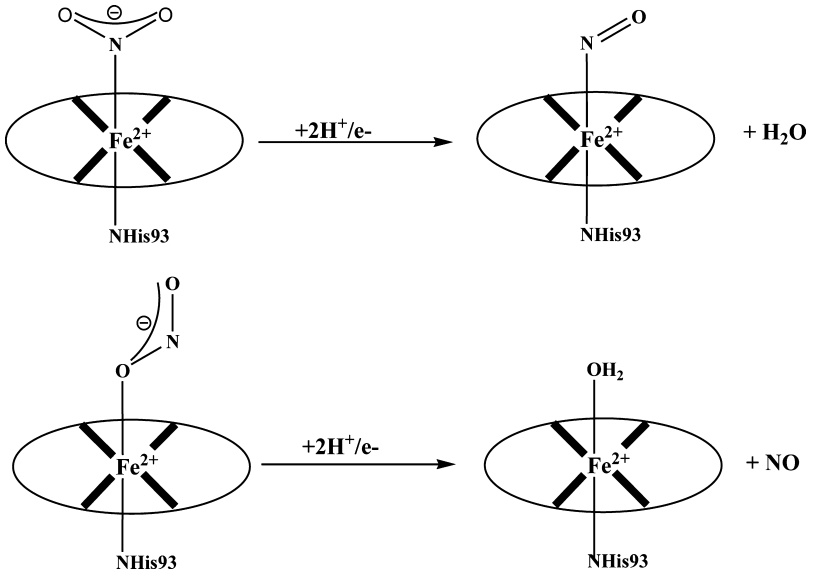

basis of EPR measurements, Schwab et al.[11a] report rhombic *g*-values for nitrite binding to methemoglobin, which are typical for N-coordinated ligands found in other heme proteins. In fact, Schwab et al.[11a] proposed that "calculations of the g-values for the different species may be very illuminating." Recently, Bawn et al. also predicted a rhombic *g*-tensor for nitrite bound myoglobin.[11b]

Density functional theory (DFT) based calculations on models of nitrite bound to ferric heme model systems predict the $-NO_2^-$ form to be slightly more stable (by 3−6 kcal mol^{-1}) as compared to the crystallographically implied $-ONO^-$ form.[12] From the mechanistic perspective, several studies are available that report reactivities such as oxene atom transfer[12c] and the formation of NO[12b] and N_2O_3 from Fe(III)-nitrite.[12d] One electron reduction of Fe(III)-nitrite leads to the formation of Fe(II)-nitrite. Crystallographically, O-binding is observed in both oxidation states.[7c] As noted by Perissionotti et al. that if $-NO_2^-$ is bound to Fe(II), the reaction may proceed via the Fe(II)NO species, whereas if $-ONO^-$ is bound to Fe(II), the reaction product is more likely to be Fe(II) bound $-OH^-$ or H_2O[12b] (Scheme 1). Thus, it is essential to understand the electronic structure of nitrite binding to low spin ferric hemes, which can consequently alter the course of the biochemical reaction.

However, to our knowledge, the computation of spin Hamiltonian (SH) parameters of low spin Fe(III)-nitrite in both linkage isomeric forms was not investigated, although such a study is important to reveal the electronic and geometric structure of potential reaction intermediates. Such studies have been reported for Fe-NO[13] species but to the best of our knowledge not for ferric-nitrites. In this Article, we have carried out both DFT and correlated *ab initio* calculations to elucidate the unique electronic structure of low spin ferric-nitrite. The nitrite coordination to the ferric heme site of both hemoglobin and myoglobin is very similar, and O-binding is found in the X-ray structures; thus, we have taken nitrite bound myoglobin for the present study.

As low spin ferric compounds have nearly orbitally degenerate $^2T_{2g}$ derived ground states, the computation of the EPR *g*-tensor is best based upon quasi-degenerate perturbation theory in a multireference *ab initio* context. In this way, the all-important spin−orbit coupling (SOC) interaction between the three components of the $^2T_{2g}$ state is treated to all orders. We show below that our computed SH parameters (such as *g*-tensor and nitrogen hyperfine coupling constants (HFCC)) are close to the experimental estimates[11b] and allow for a clear distinction between the two linkage isomeric species. Our calculations predict that O-binding of nitrite to ferric heme is modulated by His64, which alters the splitting pattern of the metal t_{2g} based orbitals that largely influence the *g*-tensor. To the best of our knowledge, this is the first computational investigation that provides direct evidence for the experimentally observed O-binding of nitrite to hemes.

2. COMPUTATIONAL DETAILS

2.1. Choice of Models. The starting structure is generated using the X-ray crystal structure[7a] of nitrite bound myoglobin (PDB Code: 2FRF, resolution = 1.20 Å). The active site consists of a heme, proximal histidine (His93), and the strong π-acceptor nitrite ligand bonded perpendicular to the heme. In addition to first coordination shell, a histidine residue (often denoted as distal His64) in close proximity can interact with nitrite through a hydrogen bond (Figure 1).

To quantify the decisive role played by distal His64, we have considered models of two different sizes (denoted as small model

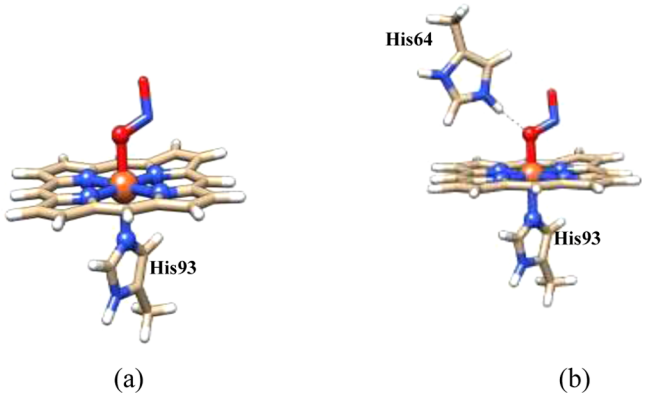

Figure 1. Chosen models: (a) small model and (b) big model of nitrite bound ferric myoglobin..

DOI: 10.1021/acs.inorgchem.5b00557
Inorg. Chem. 2015, 54, 7209−7217

Table 1. Calculated Geometric Parameters (in Å) and Relative Free Energies (kcal mol^{-1})

	small model		big model		X-ray	
X	Fe-X	Fe-N_{His93}	Fe-X	Fe-N_{His93}	Fe-X	Fe-N_{His93}
			Bond Lengths			
NO_2	1.950	2.097	1.950	2.092	2.0[2c]	2.1[2c]
ONO_T	1.872	2.060	1.896	2.043	1.94 (2.0)[7a]	2.1 (2.0)[7a]
ONO_C	1.930	2.061	1.934	2.059	2.1[7b]	2.0[7b]
			Relative Free Energies			
	small model			big model		
	NO_2	ONO_T	ONO_C	NO_2	ONO_T	ONO_C
BP86	0	+6.99	+4.71	0	+6.75	+4.74
B3LYP	0	+2.38	+2.08	0	+1.91	+1.57

Values in brackets are for the X-ray structure of 2FRI.

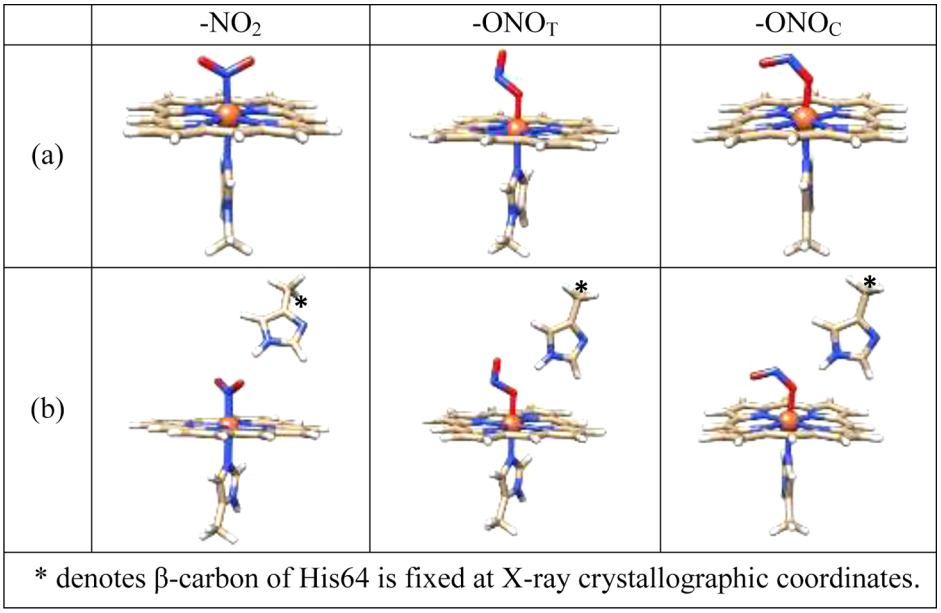

Figure 2. Optimized structures (BP86/TZVP) of (a) small model and (b) big model of nitrite-Mb.

without distal His64 and big model with distal His64, Figure 1). We have considered nitrito binding in two different orientations (denoted as -ONO_T and -ONO_C) as both species are crystallographically observed.[7b]

We have modeled the heme group as a porphinato dianion (terminal substituents are stripped). The proximal and distal histidines (His93 and His64) are modeled as methyl imidazole (truncated between C^{β}-C^{α}). Iron-porphyrin models are widely used and adequate to describe the electronic structure of iron-heme metalloproteins.[12−14] All structures are optimized using the BP86 density functional[15,16] in conjunction with the TZVP basis set[17,18] for all atoms. To mimic the protein environment, the C^{α}-carbon of His64 in the big model is fixed at the X-ray crystallographic position. In our recent study of nitric oxide bound reduced Mb (MbNO),[12a] we have used a model of larger size by incorporating His64, Val68, and Lys45. However, the role of His64 is much more dominant and alters the electronic structure more than other residues; thus, we have incorporated only His64 in the big model.

We have calculated the relative energies using both B3LYP[19,20] and BP86 functionals in conjunction with a somewhat bigger basis set for Fe═TZVPP, N, and O═TZVP and C and H═SVP. This combination of basis sets is sufficient to describe the electronic structure of iron-heme and nonheme systems.[21] Analytic vibrational frequency calculations (using AOFORCE module) are carried out on the optimized structures of SM1 to characterize the structure as minima. All geometry optimizations and frequency calculations are carried out using TURBOMOLE, version 6.0.[22] All relative energies and calculations of spin Hamiltonian parameters are carried out with ORCA 2.9.1 and 3.0.[23]

2.2. Spin Hamiltonian Calculations. EPR and MB calculations are carried out at the DFT level using the B3LYP functional.[24] For these calculations, we used a CP(PPP)[25a] (for Fe) and TZVP (for all atoms) basis set. The integration accuracy for Fe was additionally increased. EPR properties were predicted using coupled perturbed Kohn−Sham theory for the *g*-tensor[26] and the spin orbit coupling (SOC) operator was treated by spin−orbit mean-field (SOMF) approximation to the Breit-Pauli operator.[26] Fermi contact terms and spin-dipole contributions to the hyperfine coupling contributions were obtained as expectation values over the B3LYP ground state spin density. First-order hyperfine couplings were calculated for ^{1}H and ^{14}N, while spin−orbit contributions[26a] were taken into account for Fe.[26b] Isomer shift (δ) and quadrupolar splitting (ΔE_q) calculations are carried out using the expressions in ref 26. Other popular functionals such as BP86, M06-L, PBE, and TPSSh were also used to compute the SH parameters (Table S2 and S3, Supporting Information). It is shown there that the M06-L functional severely underestimates the *g*-tensor values. Furthermore, the use of the solvation model using COSMO (with ε = 5 and B3LYP functional) does not change the predicted SH parameters appreciably as compared to the corresponding gas phase value.

2.3. *Ab Initio* Calculations. Because of the nearly orbitally degenerate $^{2}T_{2g}$ ground state, we have used Complete Active Space

DOI: 10.1021/acs.inorgchem.5b00557
Inorg. Chem. 2015, 54, 7209−7217

Self Consistent Field (CASSCF) wave function by choosing five d-electrons and five d-orbitals CAS(5,5). A larger active space CAS(9,7) which consist of the sigma-bonding of coordinated heme, His93, and nitrite nitrogens are used in addition to the five d-orbitals (Figure S1, Supporting Information). It should be noted that the active space chosen here (CAS(5,5) and CAS(9,7)) is quite adequate for the calculation of *g*-tensor.[27] To recover the dynamic correlation, the systems are treated by means of N-Electron Valence State Perturbation Theory (NEVPT2).[28] The NEVPT2 method is a multiconfigurational perturbation approach based on a zeroth-order description that is provided by a complete active space self-consistent field (CASSCF) wave function. Thus, NEVPT2 derived results are comparable to the popular CASPT2 method of Roos and co-workers.[29]

3.0. RESULTS AND DISCUSSION

3.1. Structures and Energetics. Our calculated Fe−O_{ONO} bond distance (for both small- and big models, Table 1, Figure 2) of the *trans* isomer is shorter as compared to the Fe−N_{NO2} by 0.08 Å which is consistent with X-ray data[4] and with earlier computational studies.[12a,d] For the big model, a small increase in the Fe−O_{ONO} bond distance is noted (by 0.02 Å) due to the strong hydrogen bonding of a nitrito ligand with distal His64 (2.102 Å). Our optimized structures and relative energies follow a trend close to those observed by Perissinotti et al.,[12b] Silaghi-Dumitrescu,[12a] and Berto and Lehnert[12d] using other functionals. Thus, the optimized structures are not overly functional/basis set dependent.

As far as relative free energies (thermodynamic corrections are included) are concerned, we find that −NO_2 binding is favorable as compared to both −ONO binding to the Fe center in both small and big models using BP86 (by ∼7 kcal mol^{-1}) and B3LYP functionals (by ∼3 kcal mol^{-1}) (Table 1). Even after incorporation of nonthermal (zero point effects) and thermal corrections (free energies), we note that relative energy trends remain the same.[30]

Further, the calculated N═O asymmetric stretching frequencies using SM (1427 cm^{-1} (BP86/TZVP) vs 1396 cm^{-1} (FT-IR))[8d] of the Fe-NO_2 isomer is significantly red-shifted as compared to the Fe-ONO_T isomer (1530 cm^{-1} (BP86/TZVP) vs 1475 cm^{-1} (FT-IR)).[8d] A shift of ∼100 cm^{-1} may well be used as a vibrational marker to distinguish the two linkage isomers, as previously observed by Kurtikyan et al.[8d]

3.2. MB Spectroscopy. Since the relative energetics showed that the various linkage isomers are close enough in energy that under suitable circumstances any of them might be observable, we turned our attention to the computation of SH parameters derived from MB and EPR spectroscopy. The theoretical computation of MB parameters have been successfully used in the past to elucidate the electronic and geometric structures of many iron containing compounds including orbitally almost degenerate low-spin ferric hemes ($S = 1/2$).[25] We have computed the isomer-shift (δ) and quadrupole splitting (ΔE_q) of all six structures using the B3LYP functional (Table 2). It should be noted that the B3LYP functional tends to provide fairly accurate MB parameters for a large variety of iron complexes.[25]

Although the computed MB parameters for Fe−N_{NO2}^- are very close to the reported experimental data of synthetic models,[9b] the computed MB parameters for the other linkage isomer (Fe−O_{ONO}) are quite similar. Furthermore, due to the lack of experimental data for the Fe-$_{ONO}$ isomer, we cannot conclusively distinguish the linkage isomers on the basis of their MB parameters. Hence, we turned our attention toward EPR parameters.

Table 2. Computed Isomer Shift (δ) and Quadrupolar Splitting (ΔE_q in mm/s)

	-NO_2		-ONO_T		-ONO_C	
	δ	ΔE_q	δ	ΔE_q	δ	ΔE_q
small model	0.267	2.327	0.255	2.367	0.296	2.485
big model	0.251	2.539	0.255	2.486	0.280	2.593
expt[9b]	0.26	2.2				

3.3. EPR Spectroscopy. The experimental EPR spectrum has a very strong rhombic *g*-tensor whose *g*-values are typical for low spin ferric hemes ($g_{min} < 2$, $g_{mid} > \sim 2.2$, and $g_{max} > 2.8$).[10b,11] As expected, routine DFT calculations using a B3LYP functional and other functionals failed to reproduce the experimentally observed rhombic *g*-values (Tables S1 and S2, Supporting Information). Even after incorporating the solvent effects through the COSMO solvation model ($\varepsilon = 5$), the computed *g*-values failed to match the experimental values (Table S2, Supporting Information). This is partially due to the shortcomings of DFT itself in this area but mostly arises from the shortcomings of a linear response treatment that breaks down in the presence of near orbital degeneracies.[27] In this situation, it is crucial to proceed to methods that provide an infinite order treatment of the SOC. A suitable method that has provided excellent results for many orbitally near degenerate iron compounds[31] consists of the state-averaged CASSCF (SA-CASSCF) method followed by a second-order perturbation treatment of the dynamic electron correlation (NEVPT2) and quasi-degenerate perturbation theory (QDPT) for the incorporation of SOC effects. Thus, at the CASSCF and at NEVPT2 levels, all six models with CAS(5,5) and CAS(9,7) predict highly rhombic *g*-values. Furthermore, both −NO_2 and-ONO_T of SM predict *g*-values close to the experimental data. However, for the big model (Table 3), the computed *g*-tensor using the

Table 3. Computed *g*-Values and $^2T_{2g}$ Excitation Energies (cm^{-1}) for the Big model Using NEVPT2 (9,7)

	g_{min}	g_{mid}	g_{max}	$E_0 \rightarrow E_1$	$E_0 \rightarrow E_2$
			Small Model		
-NO_2	1.399	2.331	3.339	1046	2319
-ONO_T	1.751	2.263	2.882	1598	3624
-ONO_C	0.106	1.180	4.300	588	2750
			Big Model		
-NO_2	0.897	2.344	3.598	835	1787
-ONO_T	1.730	2.309	2.879	1566	3339
-ONO_C	0.874	1.867	3.864	718	2701
Expt[11b]	1.45	2.304	2.870		

−ONO_T structure matches the experimental data very closely (1.730, 2.309, and 2.879),[11] thus further distinguishing the −NO_2 and −ONO binding mode to hemes. The −ONO_C binding mode leads to g_{min} (<1) and g_{mid} (<2) values that are too low and a very large g_{max} (>3.8) that is too high relative to experiment.

The origin of different *g*-values for the three linkage isomer arises from strong coupling of the ground state with the low lying components of the low-symmetry split $^2T_{2g}$ state.[32] The intra-$^2T_{2g}$ excitation energies (Table 3) are a measure of near-degeneracy of SOMO present in the three isomers. The NEVPT2 calculations on the big model predict the first excited state of the −NO_2 and −ONO_c isomers to be nearly degenerate ($E_0 \rightarrow E_1 < 840$ cm^{-1}), whereas for the −ONO_T isomer, the

DOI: 10.1021/acs.inorgchem.5b00557
Inorg. Chem. 2015, 54, 7209−7217

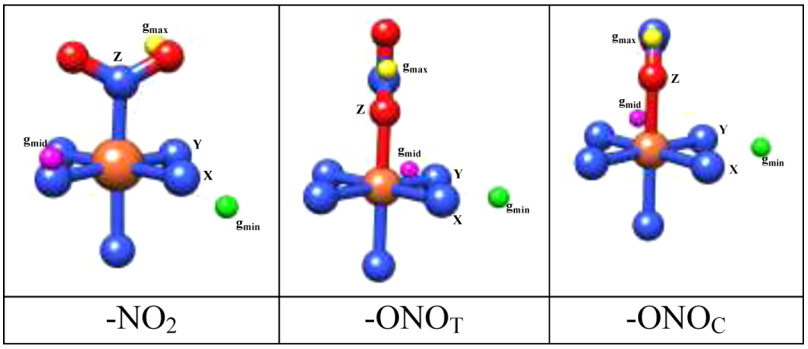

Figure 3. g-Tensor orientation. g_{min} is in green, g_{mid} in magenta, and g_{max} in yellow.

Table 4. Computed HFCC Parameters (MHz) Using the B3LYP Functional

	small model			big model			
	$-NO_2$	$-ONO_T$	$-ONO_C$	$-NO_2$	$-ONO_T$	$-ONO_C$	Expt[11b]
$^{Azz}N_{NO2}$	−20.4	−5.6	−6.7	−19.1	−1.2	−3.3	0.81
$^{Aiso}N_{Heme}$	−7.3	−6.9	−7.7	−7.3	−7.0	7.5	−7
$^{Aiso}N_{His93}$	−1.7	−6.3	−4.0	−3.7	−7.1	−6.9	−7
$^{Azz}H_{His64}$				1.7	2.9	3.3	-NA-

degeneracy is significantly lifted ($E_0 \rightarrow E_1 > 1500$ cm^{-1}). Similarly, the second excited state for $-NO_2$ and $-ONO_c$ lies fairly close ($E_0 \rightarrow E_2 < 2750$ cm^{-1}) as compared to those of $-ONO_T$ isomer (($E_0 \rightarrow E_2 > 3600$ cm^{-1}). These variations lead to very large rhombic g-tensor splitting for the $-NO_2$ and $-ONO_c$ isomers, whereas for ONO_T the g-values are still rhombic but much more narrowly spaced. In all cases, the g_{max} tensor orientation is perpendicular to the heme, whereas the g_{min} and g_{mid} g-tensor components lie in the heme plane, consistent with the available EPR data[10] (Figure 3).

To gain further insights into this intriguing system, we have computed the nitrogen HFCCs using the B3LYP functional. Although the g-tensors are not well reproduced by the B3LYP functional due to the shortcomings of the linear response formalism, ligand HFCC of nitrogen ligands should be fairly reproduced by the calculations since they represent a first-order property[33] (Table 3). Other commonly used DFs were also tested (Table S3, Supporting Information) but do not change the trends significantly. We predict a very large isotropic HFCC for $A_{zz}(N_{NO2})$ (∼20 MHz), whereas for the ONO_T species, this value is very small (∼1 MHz). Our predicted value for the HFCC of nitrite bound nitrogen is very close to the experimental estimate of 0.81 MHz obtained through HYSCORE spectroscopy (Table 3).[11b] The very large nitrogen HFCC of the nitro linkage isomer (∼20 MHz) is largely due to the direct interaction of the nitrogen atom with ferric iron, whereas in nitrito form, it is the oxygen which directly interacts with the metal center. Hence, little spin density accumulates at the nitrogen, which leads to a small ^{14}N-HFCC (∼1 MHz).

Similarly, we have also predicted the HFCCs of the heme nitrogens and the proximal His93. Although the isotropic HFCC for N_{heme} is very similar for all three species (∼7 MHz), significantly larger values are reported for N_{His93} in the $-ONO_T$ isomer (7 MHz) as compared to the $-NO_2$ isomer (Table 4). In addition, the proton attached to His64 is involved in hydrogen bonding with nitrite (2.102 Å for $ONO_{(T)}$). For *-cis* and *-trans* nitrito bound hemes, the computed HFCC of the proton of hydrogen bonded His64 is approximately twice as large as that of the nitro-bound system (Table 3). These variations confirm that the hydrogen bonding interaction is stronger for the nitrito form compared to the nitro-form.

It should be noted that between the two models, the HFCC parameters predicted using the big model agree more closely with the experimental estimates as compared to the small model. For instance, the $A_{zz}(N_{ONO})$ is larger for the small model as compared to the big model (−5.6 MHz vs −1.2 MHz). The experimental estimate of 0.81 MHz[11b] is in excellent agreement with our result for the big model. The decrease in the HFCC relative to the small model is caused by the strong hydrogen bonding present between nitrite and His64. We have also estimated the $A_{zz}(H_{His64})$ ∼3 MHz to be significantly larger due to hydrogen bonding. This HFCC may be detected in future ENDOR or HYSCORE experiments.

We have investigated the possibility that the distal His64 residue may be protonated upon nitrite binding to hemes. The optimized structural parameters and the computed SH parameters are shown in Tables S4 and S5 (Supporting Information). As expected, the protonated distal His64 hydrogen bonds to the ONO_T isomer (H−O bond distance ∼1.62 Å) more strongly than to the neutral His64 (H−O bond distance ∼2.1 Å). The stronger interaction leads to a small elongation of $Fe-O_{ONO}$ distance by ∼0.03 Å. However, the relative energies are not altered. The computed g_2 and g_3 values are larger by ∼0.1 unit when distal histidine is protonated as compared to neutral histidine. Furthermore, the HFCC of the nitrogen of proximal histidine (His93) and the hydrogen of hydrogen bonded distal histidine (His64) are larger by 1.5 MHz for the protonated form. The computed EPR parameters are also consistent with the experimental estimates, and hence, we cannot distinguish between protonated and unprotonated forms with a high degree of confidence (Figure S2 and Table S5, Supporting Information). Hence, due to the anionic nature of nitrite, distal His64 may be protonated. Such a protonation will promote N−O bond cleavage upon enzymatic reduction.[34]

In close proximity to nitrite and the distal histidine, a hydrophobic residue, Val68, is also found whose importance was investigated. We find that the presence of this amino acid does not change either the geometry or the spectroscopic

DOI: 10.1021/acs.inorgchem.5b00557
Inorg. Chem. 2015, 54, 7209−7217

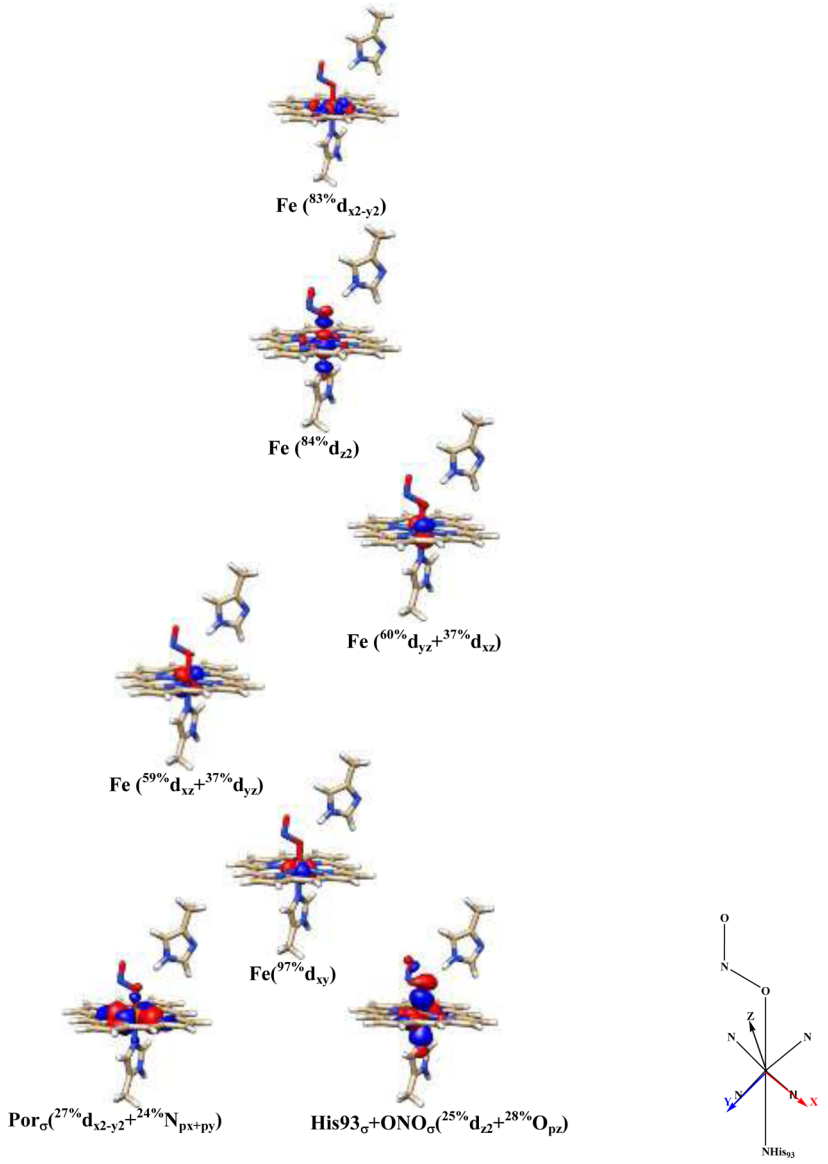

Figure 4. Electronic structure of Fe^{III}-ONO_T.

properties appreciably (Figure S3, Supporting Information). Thus, the role of distal His64 is the dominant factor, which modulates the electronic structure of low spin ferric nitrite adducts.

3.4. Electronic Structure. Our computed EPR SH parameters summarized above provide strong evidence for the O-binding of nitrite to the low spin ferric heme in the investigated systems. We can rationalize the electronic structure of this uncommon species as follows (Figure 4). On the basis of the *g*-values, the low spin ferric hemes (S = 1/2) can be classified as type-I, type-II, and type-III centers.[10b] For type-I centers, the generally observed *g*-values are g_{min} < 1, g_{mid} < 2, and "*large*" g_{max} > 3.1, whereas for a type-2 center g_{min} is between 1 and 2, g_{mid} < 2.4 and g_{max} < 3. For a type-III center, a more axial spectrum is observed ($g_{\|}$ = <2 and $g_{\perp} \sim 2.4$). This is readily explained on the basis of ligand field theory.

In octahedral symmetry, the five d-orbitals are split into t_{2g} and e_g orbitals. For low spin Fe(III) species, the five d-electrons are filling the three t_{2g}-orbitals, thus leaving one hole in the t_{2g} shell, which leads to an orbitally degenerate $^2T_{2g}$ ground state. The five d-electrons can be distributed among the three t_{2g}-based orbitals as $(d_{xy})^2(d_{xz},d_{yz})^3$ or $(d_{xz},d_{yz})^4(d_{xy})^1$. The former occupancy can lead to type-I and type-II centers, whereas the latter scenario is characteristic of type-III centers.[10]

The natural orbitals from a CAS(9,7) calculation of the big model of $Fe_{ONO(T)}$ are shown in Figure 4 (Figure S1, Supporting Information). It is evident from the plots that, as expected, the equatorial heme nitrogens and axial ligands (N_{His93} and $N_{NO2}(O_{ONO})$ form σ-bonds with the $3d_{x2-y2}$ and $3d_{z2}$ orbitals of the ferric iron which are nearly iso-energetic. Correspondingly, the antibonding $3d_{z2}$ and $3d_{x2-y2}$ orbitals form the unoccupied e_g levels. Just above the two ligand-based molecular orbitals, the doubly occupied iron-based iron $3d_{xy}$-based molecular orbital (97% iron character) is located. These three d-based orbitals (d_{xy}, d_{x2-y2}, and d_{z2}) and their ordering are very similar for all linkage isomers and are near identical for the small and big models. The remaining two d-based orbitals (d_{xz} and d_{yz}, commonly known as d_π orbitals) are different between the two linkage isomers and also differ in the small and big models.

For the small model (without His64), the two d_π orbitals are strongly mixed for the three linkage isomers. Furthermore, the

DOI: 10.1021/acs.inorgchem.5b00557
Inorg. Chem. 2015, 54, 7209−7217

excitation energy of the first excitation energy of the three isomers decreases in the following order: ONO_T > NO_2 > ONO_C (Table 3). Similarly, the second excitation energy is largest for the ONO_T, but for the ONO_C and NO_2 isomers, it differs by only 400 cm^{-1}. These variations cause smaller g_1 and very large g_3 values for ONO_C, thus leading to a type I center.

Explicitly including the distal His64 in the big model, the orbitals coefficients of the d_π orbitals and the excitation energies are modified significantly. Incorporation of His64 leads to the stabilization of the two d_π orbitals due to hydrogen bonding. In addition to this, the d_π orbitals are of essentially pure iron character (d_{yz} = 81% and d_{xz} = 82% iron character) for $-NO_2$, whereas for ONO_T, these two orbitals are mixed strongly (60% d_{yz} + 37% d_{xz} and 59% d_{xz} + 37% d_{yz}). As far as the low-lying excitation energies are concerned, the first excitation energy of ONO_T is almost unaltered (change ∼32 cm^{-1}) compared to that of the small model, whereas for the NO_2 isomer, the first excitation energy is more than 200 cm^{-1} compared to the small model. However, for ONO_C, the first excitation energy is slightly higher (∼130 cm^{-1}) compared to that of the small model. Similarly, the second excitation energies of three isomers are decreased in all three isomers. The largest changes are observed for the NO_2 isomer (stabilization by more than 500 cm^{-1}), and the smallest stabilization (∼49 cm^{-1}) is calculated for ONO_C. These subtle variations distinguish the computed *g*-tensor within the three isomers. Thus, due to the near degeneracy of ONO_C, they can be classified as type-I centers, whereas the ONO_T is of type-II *g*-tensors. Hence, all variations in the *g*-tensor can be traced back to the modulations caused by the presence of His64.

On the basis of the Taylor-Griffith simplified method for the *g*-values of a low-spin d^5 system[35] with a $^2T_{2g}$ ground state, we have calculated the ligand field parameters Δ (the energy difference between $d\pi$ orbitals) and *V* (the energy difference between d_{xy} and the barrycenter of the d_π orbitals) derived from the experimental Δg_{max} (2.870−2.002) and Δg_{mid} (2.304−2.002) shifts following ref 36. The resulting values are 876 cm^{-1} (for *V*) and 2081 cm^{-1} (for Δ). These values indicate that the intermediate orbital in ONO_T is energetically well separated, thus leading to large rhombicity. Further, the computed *V* (866 cm^{-1}) and Δ (2042 cm^{-1}) using the NEVPT2 predited *g*-shifts are also in excellent agreement with the experimentally estimated rhombicity. As the two d_π orbitals are very close in energy (<900 cm^{-1}), strong mixing of d_{yz} and d_{xz} orbitals may be expected, which is in agreement with our electronic structure calculations.

In the $-NO_2$ form, the g_{max} and g_{min} are close to type-I, whereas g_{mid} is similar to the type-II center. Furthermore, the computed nitrogen HFCCs clearly distinguishes the $-NO_2$ and $-ONO_T$ isomers. If the nitrogen of nitrite is coordinated to Fe(III), a large isotropic HFCC is expected, whereas if the binding is through O-, as in the case of $-ONO_T$ and $-ONO_C$, the HFCC of the nitrogen nucleus will be small. Indeed, our DFT calculations predicted values close to the experimental estimates of ∼1 MHz,[11b] which demonstrates that O-binding of nitrite to low spin ferric ion occurs.

4. CONCLUSIONS

In summary, through the computation of SH parameters at the correlated *ab initio* and DFT levels using models of different sizes, we have shown how the distal His64 modulates the electronic structure of nitrite adducts to low spin ferric hemes. It should be noted that frequently more than one species can be distinguished experimentally on the basis of their distinct *g*-tensor components (particularly g_{max} shows significant variations)[11a] in home-nitrite nitrite systems. These physical origins of the different *g*-tensors have been analyzed in some detail in this work and can be traced back to different orientations of nitrite relative to the heme plane. We have calculated the potential energy surface of ONO_T rotation around the heme plane for the big model (Figure S4, Supporting Information) and find that they are fairly flat (barrier of ∼5 kcal mol^{-1}). Different rotamers will alter the splitting pattern of t_{2g} orbitals and hence lead to different *g*-tensors.

In conclusion, based on the theoretical analysis of the EPR spectroscopic data, we assign the binding of nitrite to low spin ferric heme as a unique O-binding type-II center. The electronic structure elucidated here will help to better understand the mechanisms of denitrification reactions. This finding is in line with the results of Berto and Lehnert[12d] who predicted that a heme-iron−ONO^- species is essential for the formation of N_2O_3 and cannot occur for N-bound nitrite.

■ ASSOCIATED CONTENT

Supporting Information

Complete reference list of 4f, CASSCF orbitals of big models, optimized structure of big model with protonated distal His64 and with Val68, potential energy surface of nitrite rotation, computed SH parameters with different functionals and optimized structural parameters of ONO-binding with neutral and protonated His64. The Supporting Information is available free of charge on the ACS Publications website at DOI: 10.1021/acs.inorgchem.5b00557.

■ AUTHOR INFORMATION

Corresponding Author

*Tel: +91 22 25593829. Fax: +91 22 25505151. E-mail: smahesh@barc.gov.in.

Notes

The authors declare no competing financial interest.

■ ACKNOWLEDGMENTS

M.S. thanks Ajeya-Adhya systems of BARC for computing facilities. F.N. gratefully acknowledges the Max-Planck society for financial support of this work.

■ REFERENCES

(1) Ernst, K.-H.; Wild, F. R. W. P.; Blacque, O.; Berke, H. *Angew. Chem., Int. Ed.* **2011**, *50*, 10780−10787. (b) Werner, A. *Ber. Dtsch. Chem. Ges.* **1907**, *40*, 765−788.

(2) (a) Yi, J.; Safo, M. K.; Richter-Addo, G. B. *Biochemistry* **2008**, *47*, 8247−8249. (b) Novozhilova, I. V.; Coppens, P.; Lee, J.; Richter-Addo, G. B.; Bagley, K. A. *J. Am. Chem. Soc.* **2006**, *128*, 2093−2104. (c) Yi, J.; Thomas, L. M.; Richter-Addo, G. B. *Angew. Chem., Int. Ed.* **2012**, *51*, 3625−3627. (d) Kurtikyan, T. S.; Ford, P. C. *Angew. Chem., Int. Ed.* **2006**, *45*, 492−496. (e) Sanders, B. C.; Hassan, S. M.; Harrop, T. C. *J. Am. Chem. Soc.* **2014**, *136*, 10230−10233.

(3) (a) Buckingham, D. A.; Creaser, I. I.; Sargeson, A. M. *Inorg. Chem.* **1970**, *9*, 655−661. (b) Bitterwolf, T. E. *Coord. Chem. Rev.* **2006**, *250*, 1196−1207. (c) Surducan, M.; Lup, D.; Lupan, A.; Makarov, S. V.; Silaghi-Dumitrescu, R. *J. Inorg. Biochem.* **2013**, *118*, 13−20. (d) Schaniel, D.; Mockus, N.; Woike, T.; Klein, A.; Sheptyakov, D.; Todorova, T.; Delley, B. *Phys. Chem. Chem. Phys.* **2010**, *12*, 6171−6178.

(4) (a) Maia, L. B.; Moura, J. J. G. *Chem. Rev.* **2014**, *114*, 5273−5357. (b) Einsle, O.; Messerschmidt, A.; Huber, R.; Kroneck, P. M. H.;

DOI: 10.1021/acs.inorgchem.5b00557
Inorg. Chem. 2015, 54, 7209−7217

Neese, F. *J. Am. Chem. Soc.* **2002**, *124*, 11737−11745. (c) Tocheva, E. I.; Rosell, F. I.; Mauk, A. G.; Murphy, M. E. P. *Science* **2004**, *304*, 867−870. (d) Pomowski, A.; Zumft, W. G.; Kroneck, P. M. H.; Einsle, O. *Nature* **2011**, *477*, 234−237. (e) Antonyuk, A. V.; Strange, R. W.; Sawers, G.; Eady, R. R.; Hasnain, S. S. *Proc. Natl. Acad. Sci. U. S. A.* **2005**, *102*, 12041−12046. (f) Gladwin, M. T.; Schechter, A. N.; Kim-Shapiro, D. B.; Patel, R. P.; Hogg, N.; Shiva, S.; Cannon, R. O., III; Kelm, M.; Wink, D. A.; Espey, M. G.; Oldfield, E. H.; et al. *Nat. Chem. Biol.* **2005**, *1*, 308−314. (g) Komeda, N.; Hirotaka, N.; Yoshinori, K.; Gin-Ya, A.; Masatatsu, S.; Akila, U.; Koji, T. *Bull. Chem. Soc. Jpn.* **1995**, *68*, 581−589. (h) Lehnert, N.; Cornelissen, U.; Neese, F.; Ono, T.; Noguchi, y.; Okamoto, K.; Fujisawa, K. *Inorg. Chem.* **2007**, *46*, 3916−3933. (i) Woollard-Shore, J. G.; Holland, J. P.; Jones, M. W.; Dilworth, J. R. *Dalton Trans.* **2010**, *39*, 1576−1585. (j) Merkle, A. C.; Lehnert, N. *Dalton Trans.* **2012**, *41*, 3355−3368.

(5) (a) Wayland, B. B.; Olson, L. W. *J. Am. Chem. Soc.* **1974**, *96*, 6037−6041. (b) Cooper, C. E. *Biochim. Biophys. Acta, Bioenerg.* **1999**, *1411*, 290−309. (c) Stolzenberg, A. M.; Strauss, S. H.; Holm, R. H. *J. Am. Chem. Soc.* **1981**, *103*, 4763−4778.

(6) (a) Xu, N.; Yi, J.; Richter-Addo, G. B. *Inorg. Chem.* **2010**, *49*, 6253−6266. (b) Sundararajan, M.; Hillier, I. H.; Burton, N. A. *J. Phys. Chem. B* **2007**, *111*, 5511−5517. (c) Bykov, D.; Neese, F. *JBIC, J. Biol. Inorg. Chem.* **2011**, *16*, 417−430. (d) Harrop, T. C.; Song, D.; Lippard, S. J. *J. Am. Chem. Soc.* **2006**, *128*, 3528−3529. (e) Periyasamy, G.; Sundararajan, M.; Hillier, I. H.; Burton, N. A.; McDouall, J. J. W. *Phys. Chem. Chem. Phys.* **2007**, *9*, 2498−2506. (f) Olah, J.; Harvey, J. N. *J. Phys. Chem. A* **2009**, *113*, 7338−7345. (g) Radon, M.; Pierloot, K. *J. Phys. Chem. A* **2008**, *112*, 11824−11832.

(7) (a) Copeland, D. M.; Soares, A. S.; West, A. H.; Richter-Addo, G. B. *J. Inorg. Biochem.* **2006**, *100*, 1413−1425. (b) Yi, J.; Heinecke, J.; Tan, H.; Ford, P. C.; Richter-Addo, G. B. *J. Am. Chem. Soc.* **2009**, *131*, 18119−18128. (c) Yi, J.; Orville, A. M.; Skinner, J. M.; Skinner, M. J.; Richter-Addo, G. B. *Biochemistry* **2010**, *49*, 5969−5971. (d) Zahran, Z. N.; Chooback, L.; Copeland, D. M.; West, A. H.; Richter-Addo, G. B. *J. Inorg. Biochem.* **2008**, *102*, 216−233. (e) Yi, J.; Safo, M. K.; Richter-Addo, G. *Biochemistry* **2008**, *47*, 8247−8249.

(8) (a) Kurtikyan, T. S.; Ford, P. C. *Coord. Chem. Rev.* **2008**, *252*, 1486−1496. (b) Ford, P. C. *Inorg. Chem.* **2010**, *49*, 6226−6239. (c) Ford, P. C.; Lorkovic, I. M. *Chem. Rev.* **2002**, *102*, 993−1018. (d) Kurtikyan, T. S.; Hovhannisyan, A. A.; Hakobyan, M. E.; Patterson, J. C.; Iretskii, A.; Ford, P. C. *J. Am. Chem. Soc.* **2007**, *129*, 3576−3585. (e) Kurtikyan, T. S.; Hovhannisyan, A. A.; Gulyan, G. M.; Ford, P. C. *Inorg. Chem.* **2007**, *46*, 7024−7031.

(9) (a) Nasri, H.; Ellison, M. K.; Krebs, C.; Huynh, B. H.; Scheidt, W. R. *J. Am. Chem. Soc.* **2000**, *122*, 10795−10804. (b) Nasri, H.; Ellison, M. K.; Shang, M.; Schulz, C. E.; Scheidt, W. R. *Inorg. Chem.* **2004**, *43*, 2932−2942. (c) Nasri, H.; Wang, Y.; Huynh, B. H.; Walker, F. A.; Scheidt, W. R. *Inorg. Chem.* **1991**, *30*, 1483−1489. (d) Nasri, H.; Haller, K. J.; Wang, Y.; Huynh, B. H.; Scheidt, W. R. *Inorg. Chem.* **1992**, *31*, 3459−3467.

(10) (a) Walker, F. A. *Chem. Rev.* **2004**, *104*, 589−615. (b) Walker, F. A. *Coord. Chem. Rev.* **1999**, *185*−*186*, 471−534. (c) Teschner, T.; Yatsunyk, L.; Schünemann, V.; Paulsen, H.; Winkler, H.; Hu, C.; Scheidt, W. R.; Walker, F. A.; Trautwein, A. X. *J. Am. Chem. Soc.* **2006**, *128*, 1379−1389.

(11) (a) Schwab, D. E.; Stamler, J. S.; Singel, D. J. *Inorg. Chem.* **2010**, *49*, 6330−6337. (b) Bawn, J. Myoglobin and Nitrite: An Electron Paramagnetic Resonance Led Investigation. Ph.D. Thesis, University of East Anglia, U.K., 2012. (c) Gadsby, P. M. A.; Thomson, A. J. *J. Am. Chem. Soc.* **1990**, *112*, 5003−5011.

(12) (a) Silaghi-Dumitrescu, R. *Inorg. Chem.* **2004**, *43*, 3715−3718. (b) Perissionotti, L. L.; Marti, M. A.; Doctorovich, F.; Luque, F. J.; Estrin, D. A. *Biochemistry* **2008**, *47*, 9793−9802. (c) Conradie, J.; Ghosh, A. *Inorg. Chem.* **2006**, *45*, 4902−4909. (d) Berto, T. C.; Lehnert, N. *Inorg. Chem.* **2011**, *50*, 7361−7363.

(13) (a) Sundararajan, M.; Neese, F. *J. Chem. Theory Comput.* **2012**, *8*, 563−574. (b) Patchkovskii, S.; Ziegler, T. *Inorg. Chem.* **2000**, *39*, 5354−5364. (c) Radoul, M.; Sundararajan, M.; Potapov, A.; Riplinger, C.; Neese, F.; Goldfarb, D. *Phys. Chem. Chem. Phys.* **2010**, *12*, 7276−7289. (d) Radoul, M.; Bykov, D.; Rinaldo, S.; Cutruzzola, F.; Neese, F.; Goldfarb, D. *J. Am. Chem. Soc.* **2011**, *133*, 3043−3055.

(14) (a) Sigfridsson, E.; Olsson, M. H. M.; Ryde, U. *J. Phys. Chem. B* **2001**, *105*, 5546−5552. (b) Jensen, K. P.; Ryde, U. *ChemBioChem* **2003**, *4*, 413−424. (c) Schöneboom, J. C.; Neese, F.; Thiel, W. *J. Am. Chem. Soc.* **2005**, *127*, 5840−5853. (d) Vincent, M. A.; Hillier, I. H.; Ge, J. *Chem. Phys. Lett.* **2005**, *407*, 333−336. (e) Li, C.; Zhang, L.; Zhang, C.; Wu, W.; Hirao, H.; Shaik, S. *Angew. Chem., Int. Ed.* **2007**, *46*, 8168−8170.

(15) Becke, A. D. *Phys. Rev. A: At., Mol., Opt. Phys.* **1988**, *38*, 3098−3100.

(16) Perdew, J. P. *Phys. Rev. B: Condens. Matter Mater. Phys.* **1986**, *33*, 8822−8824.

(17) Schaefer, A.; Horn, H.; Ahlrichs, R. *J. Chem. Phys.* **1992**, *97*, 2571−2577.

(18) Schaefer, A.; Huber, C.; Ahlrichs, R. *J. Chem. Phys.* **1994**, *100*, 5829−5835.

(19) Becke, A. D. *J. Chem. Phys.* **1993**, *98*, 5648−5652.

(20) Lee, C.; Yang, W.; Parr, R. G. *Phys. Rev. B: Condens. Matter Mater. Phys.* **1988**, *37*, 785−789.

(21) (a) Christian, G. J.; Ye, S.; Neese, F. *Chem. Sci.* **2012**, *3*, 1600−1611. (b) Sundararajan, M.; Ganyushin, D.; Ye, S.; Neese, F. *Dalton Trans.* **2009**, 6021−6036.

(22) *TURBOMOLE, version 6.0*. University of Karlsruhe and Forschungszentrum Karlsruhe GmbH: Karlsruhe, Germany, 2009.

(23) (a) Neese, F.; Becker, U.; Ganyushin, D.; Liakos, D. G.; Kossmann, S.; Petrenko, T.; Riplinger, C.; Wennmohs, F. *ORCA, 2.9.0*; University of Bonn: Bonn, Germany, 2009. (b) Neese, F. *Wiley Interdiscip. Rev. Comput. Mol. Sci.* **2012**, *2*, 73−78.

(24) Other popular functionals such as BP86, PBE, TPSSh, and M06-L functionals were tested, and we found that the computed nitrogen HFCs are of very similar magnitude (ESI).

(25) (a) Neese, F. *Inorg. Chim. Acta* **2002**, *337*, 181−192. (b) Sinnecker, S.; Slep, L. D.; Bill, E.; Neese, F. *Inorg. Chem.* **2005**, *44*, 2245−2254. (c) Papai, M.; Vanko, G. *J. Chem. Theory Comput.* **2013**, *9*, 5004−5020. (d) Zhang, Y.; Mao, J.; Godbout, N.; Oldfield, E. *J. Am. Chem. Soc.* **2002**, *124*, 13921−13930. (e) Zhang, Y.; Mao, J.; Oldfield, E. *J. Am. Chem. Soc.* **2002**, *124*, 7829−7839. (f) Bochevarov, A. D.; Friesner, R. A.; Lippard, S. J. *J. Chem. Theory Comput.* **2010**, *6*, 3735−3749. (g) Sandela, G. M.; Hopmann, K. H.; Ghosh, A.; Noodleman, L. *J. Chem. Theory Comput.* **2011**, *7*, 3232−3247.

(26) (a) Neese, F. *J. Chem. Phys.* **2005**, *122*, 034107−13. (b) Neese, F. *J. Chem. Phys.* **2001**, *115*, 11080−11096.

(27) Neese, F. *Magn. Reson. Chem.* **2004**, *42*, S187−S198.

(28) (a) Angeli, C.; Cimiraglia, R.; Evangelisti, S.; Leininger, T.; Malrieu, J. P. *J. Chem. Phys.* **2001**, *114*, 10252−10264. (b) Angeli, C.; Cimiraglia, R.; Malrieu, J.-P. *Chem. Phys. Lett.* **2001**, *350*, 297−305. (c) Domingo, A.; Carvajal, M.-A.; de Graaf, C.; Sivalingam, K.; Neese, F.; Angeli, C. *Theor. Chem. Acc.* **2012**, *131*, 1264−1277. (d) Schapiro, I.; Sivalingam, K.; Neese, F. *J. Chem. Theory Comput.* **2013**, *9*, 3567−3580. (e) Neese, F.; Liakos, D. G.; Ye, S. *JBIC, J. Biol. Inorg. Chem.* **2011**, *16*, 821−829. (f) Duboc, C.; Ganyushin, D.; Sivalingam, K.; Collomb, M. N.; Neese, F. *J. Phys. Chem. A* **2010**, *114*, 10750−10758.

(29) (a) Andersson, K.; Malmqvist, P. A.; Roos, B. O.; Sadlej, A. J.; Wolinski, K. *J. Phys. Chem.* **1990**, *94*, 5483−5488. (b) Vancoillie, S.; Malmqvist, P.-A.; Pierloot, K. *ChemPhysChem* **2007**, *8*, 1803−1815.

(30) We have also calculated the relative energies with approximate protein effects using the COSMO solvation model (with $\varepsilon = 5$), with the dispersion effect using the D3-BJ correction on B3LYP functional. Even after incorporation of these dispersion and solvent effects, the relative energy trends remain the same (Tables S2 and S3, Supporting Information). Other popular functionals such as M-06L and TPSSh functionals are also used, which does not change the relative energetics. Further, we have also used a bigger basis set (TZVPP for Fe and TZVP for all other atoms), which does also not alter the overall relative energetics.

(31) (a) Atanasov, M.; Zadrozny, J. M.; Long, J. F.; Neese, F. *Chem. Sci.* **2013**, *4*, 139−156. (b) Zadrozny, J. M.; Xiao, D. J.; Atanasov, M.; Long, G. J.; Grandjean, F.; Neese. *Nat. Chem.* **2013**, *5*, 577−581.

DOI: 10.1021/acs.inorgchem.5b00557
Inorg. Chem. 2015, 54, 7209−7217

(32) van Gastel, M.; Lubitz; Lassmann, G.; Neese, F. *J. Am. Chem. Soc.* **2004**, *126*, 2237−2246.
(33) (a) Sinnecker, S.; Neese, F. *J. Comput. Chem.* **2006**, *27*, 1463−1475. (b) Neese, F. *J. Phys. Chem. A* **2001**, *105*, 4290−4299. (c) Neese, F. *JBIC, J. Biol. Inorg. Chem.* **2006**, *11*, 702−711. (d) Munzarova, M.; Kaupp, M. *J. Phys. Chem. A* **1999**, *103*, 9966−9983. (e) Jayapal, P.; Rajaraman, G. *Phys. Chem. Chem. Phys.* **2012**, *14*, 9050−9053.
(34) Bykov, D.; Neese, F. *JBIC, J. Biol. Inorg. Chem.* **2011**, *16*, 417.
(35) Taylor, C. P. S. *Biochim. Biophys. Acta, Protein Struct.* **1977**, *491*, 137.
(36) Neese, F.; Zaleski, J. M.; Zaleski, K. L.; Solomon, E. I. *J. Am. Chem. Soc.* **2000**, *122*, 11703.

DOI: 10.1021/acs.inorgchem.5b00557
Inorg. Chem. 2015, 54, 7209−7217